The Study of Chiral Adsorption Systems using Synchrotron-based Structural and Spectroscopic Techniques: Stereospecific Adsorption of Serine on Au-Modified Chiral Cu{531} Surfaces

Tugce Eralp, Alix Cornish, Andrey Shavorskiy

Georg Held*

University of Reading, Department of Chemistry, Whiteknights, Reading, UK

Revised Manuscript July 20, 2011

* **Corresponding address:**

University of Reading, Department of Chemistry

Whiteknights, Reading RG6 6AD UK

Email: g.held@reading.ac.uk

Abstract

We apply modern synchrotron based structural techniques to the study of serine adsorbed on the pure and Au-modified intrinsically chiral Cu{531} surface. XPS and NEXAFS data in combination with DFT show that on the pure surface both enantiomers adsorb in μ_4 geometries (with de-protonated β-OH groups) at low coverage and in μ_3 geometries at saturation coverage. Significantly larger enantiomeric differences are seen for the μ_4 geometries, which involve substrate bonds of three side groups of the chiral center, i.e. a three-point interaction. The μ_3 adsorption geometry, where only the carboxylate and amino groups form substrate bonds, leads to smaller but still significant enantiomeric differences, both in geometry and the decomposition behavior. When Cu{531} is modified by the deposition of 1 and 2 ML Au the orientations of serine at saturation coverage are significantly different from those on the clean surface. In all cases, however, a μ_3 bond coordination is found at saturation involving different numbers of Au atoms, which leads to relatively small enantiomeric differences.

1 Introduction

It was first pointed out by Easson and Stedman in 1933 that chiral recognition requires a three-point interaction of the reactant molecule i.e. three side groups of the chiral center have to be held in place by specific interactions with its environment [1]. More recently, Davankov pointed out that these interactions can either be attractive or repulsive [2]. This poses one of the great challenges in designing heterogeneous enantioselective catalysts as a two-dimensional solid surface needs to be functionalized such that it confines the three respective side groups of a chiral (or prochiral) molecule, which are not normally accessible in the same plane. The most successful strategies for achieving this goal so far involve "adding a third dimension" to the catalyst surface, either by immobilizing homogeneous catalysts, which themselves provide a three-dimensional cage for the reactant and use the catalyst surface only as anchor point [3] or by employing large modifier molecules, which create a stereoselective environment together with the surface [4, 5]. In the latter case the catalyst surface accounts for one or two of the interactions. In addition, enantioselectivity has also been observed in the adsorption behavior of a variety of molecules on intrinsically chiral model catalyst surfaces [6, 7, 8, 9]. These are single crystal metal surfaces without mirror symmetry, which are not superimposable onto their mirror images [10, 11, 12]. In the past, studies of enantioselective behavior on these surfaces have been largely based on adsorption/desorption experiments, either in vacuum, using temperature programmed desorption (TPD) [13, 14, 15, 16], or in solution, using cyclovoltammetry [17, 7, 18]. By comparing the behavior of different intrinsically chiral surfaces, Attard et al. found a correlation between the degree of enantioselectivity in electrooxidation reactions and the density of low-coordinated kink atoms on the electrode surface [7] and similar correlations were found in TPD experiments by Gellman et al. [15]. The exact nature of the interaction between adsorbates and these kink sites was, however, not clear nor is there an obvious rule under which circumstances the interaction with chiral molecules leads to the stabilization

of (R)/(R) or (R)/(S) combinations.

More detailed crystallographic information about the number and nature of enantiospecific interactions between chiral adsorbates and a metal surface emerged over the last few years, both from theory and experiment [19, 20, 21, 22, 23, 24, 25, 26, 27]. The first combination of experimental and theoretical work in this context was a combined DFT and photoelectron diffraction study of enantioselective effects in the adsorption geometry of cysteine on Au{17 11 9} by Greber et al. [22]. This study identified the steric repulsion of the carboxylic acid group as one of the three interactions necessary. The general problem in determining structural features of chiral surface systems experimentally is their complexity and often a lack of long-range order. For this reason synchrotron-based methods have often been more successful than the generally more precise technique of low-energy electron diffraction (LEED). Using element-specific photoelectron emission or photoabsorption as a local probe enables the determination of certain parameters of the adsorption geometry in the vicinity of the emitter/absorber atom without having to consider the long-range environment. Modern third-generation synchrotron radiation sources provide excellent beam quality in terms of brilliance, energy resolution and polarization and are now widely available to be used for catalysis-related research.

In this article we will give a brief overview over the main synchrotron-based techniques available and compare them with other structural techniques. As a model system we concentrate on the adsorption of serine, on the pure and Au-modified intrinsically chiral Cu{531} surface (see Fig. 1). In contrast to glycine and alanine [24, 27], serine can form bonds with the Cu surface through either two or three side groups of the chiral center, depending on coverage. We have shown that attractive interactions of all three side groups lead to large enantiomeric differences in the adsorption geometries and energies of serine, whereas two strong attractive interactions combined with a repulsive interaction or a weak hydrogen bond cause significantly weaker but still significant enantioselective effects [28]. In the latter case the adsorption "footprint" is similar to alanine and also the enantiomeric

differences are comparable. Cu{531} has the smallest surface unit cell of all intrinsically chiral Cu surfaces, which makes it readily accessible for DFT and LEED-IV structural analysis. Chemical modification is achieved by depositing gold layers of 1 and 2 ML thickness.

2 Experimental Techniques

The general problem in determining structural features of chiral surface systems experimentally lies in their complexity and often a lack of long-range order. The synchrotron-based methods discussed below utilize element-specific photoelectron emission or photoabsorption as local probes, which enable the determination of certain parameters of the adsorption geometry in the vicinity of the emitter/absorber atom without having to consider the long-range environment.

2.1 Diffraction Techniques: X-ray Photoelectron Diffraction

Determining the complete geometry of the adsorption complex of medium-size molecules on intrinsically chiral surfaces is a serious challenge for established surface crystallography techniques, such as quantitative low energy electron diffraction (LEED-IV) or surface X-ray diffraction. The structures of several unreconstructed clean surfaces have been determined over the last few years by LEED-IV and density functional theory (DFT) with good agreement between experiment and theory [29, 30, 31].

So far, complete experimental structure determinations (adsorbate conformation and registry with underlying substrate) have not been carried out for chiral molecules adsorbed on intrinsically chiral surfaces. However, synchrotron-based photoelectron diffraction has been used to extract partial structural information from chiral adsorption systems, such as cysteine on Au{17 11 9} [22] (molecular conformation), and alanine or tartaric acid on Cu{110} [32, 20] (positions of bond-forming atoms). In the kinetic energy range of soft X-

ray photoelectrons, typically several hundred eV, the De Broglie wave length of electrons is of the order of 1 Å. Therefore, photoelectrons that are scattered by atoms surrounding the emitter atom can interfere with the directly emitted electron wave and lead to significant intensity variations as function of detection angle and kinetic (photon) energy. These photoelectron diffraction effects strongly depend on the position of the scattering atoms with respect to the emitter and can, thus, be used as a tool to determine the surface structure [33, 34, 35]. The particular advantage of photoelectron diffraction over other surface-sensitive diffraction methods, such as LEED and surface X-ray diffraction, is that it is element specific (only one photoelectron emission line is used and the environment of the corresponding atoms is probed) and does not require long range order (the only condition is that the local environment must be the same for all emitter atoms).

For kinetic energies higher than about 400-500 eV electrons are predominantly scattered in the forward direction [36]. This leads to the so-called "forward focussing effect" when another atom is between the emitter and the detector. In this direction the intensity is amplified, whereas small intensity minima are observed at angles 10-20° away from this direction. The maxima in the angular distribution of the photoelectron intensity, therefore, correspond directly to the connecting lines between the emitter and neighboring atoms, which makes the data analysis straight-forward.

For energies below 300 eV elastic scattering away from the forward direction is very significant, whereby backscattering is a particularly important scattering path. The photoelectron signal emitted from adsorbate atoms is therefore the superposition of the direct wave and the electron wave back-scattered from the substrate atoms. The interference of these two waves carries information about the registry between adsorbate and substrate, i.e. adsorption sites and adsorbate-substrate bond lengths, which is not accessible with higher kinetic energies. Scanning the photon energy with the detector recording the photoelectron signal at a fixed angle has become the standard way of data acquisition for this technique. The photon energy range is chosen such that the kinetic energy of the

photoelectrons varies between typically 20 and 300 eV. Therefore, these measurements can only be performed at synchrotrons.

Modeling using DFT is an alternative way of structure determination. The adsorption geometries for a large number of medium-size chiral molecules on intrinsically chiral metal surfaces have been optimized this way [37, 38, 21, 23, 22, 25, 26, 28] but the energy differences between different conformations are often well within the error margin of DFT, about 0.1 eV, so that independent experimental data are necessary for unambiguous results. Despite its great success in determining local chiral arrangements at the molecular level [39], scanning tunneling microscopy (STM) is of little use for determining the exact adsorption geometry at the atomic level in terms of bond coordination and the orientation of sub-molecular side groups. DFT modeling of STM height maps and comparison with experimental data can reveal information about the intra-molecular geometry in certain cases (see e.g. [40]) but the assumptions made in this approach, most notably about the state of the STM tip cannot always be verified experimentally.

2.2 Spectrocopic Techniques: XPS, NEXAFS - Bond Coordination and Molecular Orientation

In addition to diffraction techniques, spectroscopic techniques can be used to determine the bond coordination and/or orientation of single atoms of functional groups in many cases where an absolute determination of atom positions or interatomic bond lengths with crystallographic methods is not possible. Reflection absorption IR spectroscopy (RAIRS) has been extensively used to characterize the symmetry and coordination of adsorption complexes of a large number of chiral molecules on achiral single crystal surfaces (for recent reviews see Refs. [39, 41]). Experimental data can be compared with a large data base of spectra from organometallic complexes which is particularly useful for assigning specific side groups, e.g. COOH vs COO^- or NH_2 vs NH_3^+, determining the bond coordination, and identifying hydrogen bonding. The only major problem is that vibrations parallel to

metal surfaces cannot be observed due to cancelation by the image dipole.

High-resolution X-ray photoelectron spectroscopy (XPS) has similar capabilities as RAIRS in terms of discriminating between the chemical state of particular side groups and determining the bond coordination on the basis of chemical shifts of core level binding energies (BE). For amino acids there exists now a reliable data base for comparison [42, 43, 44, 45, 24, 46, 47, 48, 27, 49, 50]. De-protonated carboxylate groups which form a bond with the metal surface lead to a single O 1s peak around 531.5 eV and a C 1s peak around 288 eV, whereas the backbone carbon atoms in chemisorbed layers give rise to XPS intensity in the BE region between 285 and 286 eV. The N 1s spectral region allows a straight-forward discrimination between NH_2 (BE $\approx$ 400 eV) and zwitterionic NH_3 (BE $\approx$ 402 eV). Decomposition products usually give rise to signals at lower BE, whereas atoms in multilayers have higher XPS binding energies. In particular, the XPS signal of not surface-bound intact OH groups is usually found around 533 eV. Serine has three functional groups (COOH, NH_2, and β-OH), which can thus be readily identified by XPS. One particular advantage of XPS is that it is a quantitative technique. Care needs to be taken, however, to avoid beam damage, especially when the experiments are carried out at high-brilliance third-generation synchrotron facilities.

Near-edge X-ray absorption fine structure (NEXAFS) spectroscopy has proven to be a useful technique for determining the orientation of specific side groups by making use of the polarization dependence of absorption resonances. According to the dipole selection rule, the absorption cross-section for an excitation from an atomic s orbital into an unoccupied molecular π orbital varies like $\cos^2(\phi - \alpha)$, where $(\phi - \alpha)$ is the angle between the polarization vector and the normal to the plane or axis of symmetry of the orbital [51]. Chemisorbed amino acids usually have a de-protonated carboxylate group with a localized π^* orbital giving rise to sharp resonances in C and O K-edge NEXAFS spectra at photon energies around 289 eV and 533 eV, respectively. By rotating the sample with respect to the linear polarization of the incoming X-ray beam (or vice versa) the angle α can be

varied and, hence, the orientation of carboxylate group can be determined with respect to the known crystallographic orientation of the substrate [27, 24, 45, 42, 52]. The intensity of the π-resonance peak is expected to go to zero if the polarization vector, $\vec{E}$, is in the plane of the O-C-O triangle and should have maximum intensity if $\vec{E}$ is perpendicular to this plane. A low-symmetry surface like Cu{531} allows the determination of the in-plane orientation by rotating $\vec{E}$ within the surface plane. This is not possible for surfaces with three- or four-fold symmetry. When multiple molecular orientations are present in the adsorbate layer, the intensity of the π-resonance from each molecular orientation varies like $cos^2(\phi - \alpha_i)$, where α_i is the angle between an arbitrary x-axis within the surface (in the present work we choose the $[1\overline{1}2]$ direction) and the projection of the normal of O-C-O triangle (describing the orientation of the molecule) and ϕ is the azimuthal angle of the polarization vector with respect to the x-axis.

The resonance intensities for each angle ϕ are extracted by fitting the corresponding NEXAFS spectra (examples are shown in Figure 5, details of the fit procedures are described e.g. in [27]). The resulting angular dependence of the π-resonance is then fitted with a function describing the expected angular intensity dependence for molecules in different orientations. For two orientations, α_1 and α_2 the fit function is:

$$I_\pi(\phi) = \Theta_1 \cdot (cos^2(\phi - \alpha_1)) + \Theta_2 \cdot (cos^2(\phi - \alpha_2)) \qquad (1)$$

Θ_1 and Θ_2 define the relative coverages of the two molecular configurations.

2.3 Specific Experimental Details

Most of the experiments reported here were carried out at the the German synchrotron radiation facility BESSY **using the undulator beamline UE52-PGM with variable linear and circular polarization.** Sample preparation and preliminary TPD and LEED experiments were performed at the University of Reading. The experimental procedures are described in detail elsewhere [24, 27, 49]. Two Cu{531} samples with R and S chi-

rality, respectively, were used for the experiments at Reading and BESSY, the absolute chirality of which had been determined by LEED-IV [31]. Serine was deposited at a rate of typically 1 ML / 20 min from a glass crucible housed in a stainless steel tube which was resistively heated to 160°C. Gold was evaporated from a thin gold wire wrapped around a resistevely heated tungsten wire. The deposition rate for gold was 1 ML/40 s [53]. All NEXAFS experiments were performed at normal incidence, **which means that the polarization vector of the incoming X-rays was always parallel to the surface plane.** The in-plane polarization could be changed continuously between horizontal (parallel to $[1\overline{1}2]$) and vertical. C K-edge NEXAFS spectra were recorded in the partial-yield mode **(retarding voltage 210 V)** by scanning the photon energy from 286 to 320 eV. The spectra shown here are normalized with respect to the photon flux and have the spectra of the clean surface subtracted. **The monchromator readings of the photon energies were not calibrated further as the exact energies are not important for the data analysis in terms of angular dependence.** Details of the NEXAFS data analysis are described elsewhere [27, 49].

3 Serine on clean Cu{531}

When serine is deposited on the pure Cu{531} surface at room temperature in vacuum no condensation of multilayers is observed; the chemisorbed layer saturates at a coverage of 0.50 ML **(see below for justification).** Ordered LEED superstructures were observed after adsorption at room temperature for low coverages of both enantiomers, between 30% and 60% of the saturated chemisorbed layer($\approx$ 0.15 to 0.30 ML). For the saturated chemisorbed layers ordered superstructures were only obtained after heating the sample to 370 K. The LEED diffraction patterns are different for the two enantiomers indicating different long-range ordering. On Cu{531}^{R} the low-coverage superstructure of L-serine is (-1 1; -1 -2), which corresponds to a local coverage of 0.33 ML. The LEED pattern

is sharpest for low coverages but can be observed up to near the nominal coverage **of 0.33 ML**. D-serine forms a (-1 1; -2 -4) superstructure with a unit cell twice the size of L-serine (see Figure 2(a)). At saturation coverage, L- and D-serine show $p(1 \times 8)$ and $p(1\times4)$ diffraction patterns, respectively, on Cu$\{531\}^R$ with faint elongated superstructure spots after annealing, which indicate non-perfect long-range order (see Figure 2.b). For steric reasons a maximum of four/two molecules can be accommodated in the $p(1 \times 8)/p(1 \times 4)$ unit cell of the saturated L/D-serine layer, which leads to the saturation coverage of $\frac{4}{8} = \frac{2}{4} = 0.50$ ML. **Schematic models for the superstructures observed in LEED are presented in Figure 3(a)-(d) using the surface coordination and orientation derived form XPS and NEXAFS (see below for further details). It is important to note that the LEED experiments were performed on a Cu{531}^{R} surface. On the Cu{531}^{S} surface, used for the XPS and NEXAFS experiments, the superstuctures reported above are, therefore, expected for the opposite enantiomers. For better comparability with the spectroscopic data, Figure 3 represents the situation on Cu{531}^{S}. The spot shape observed in LEED for the saturated layers indicates elongated domains with better ordering along the $\vec{a}_1$ direction and less long-range correlation along $\vec{a}_2$. The round spots observed for the low-coverage structures indicate isotropic island growth.**,

The C 1s and N 1s XP spectra are in good agreement with those observed for serine on Cu{110} [49] and show little qualitative differences when the coverage or the enantiomer changes. The C 1s spectra of both enantiomers show main peaks at binding energies (BE) around 288.1 eV and 286.0 eV, Figure 4(b). The high BE signal originates from the de-protonated carboxylic acid carbon [24, 42, 45, 27]; the main peak at 286.2 eV is the overlapping signal of α and β-carbon atoms and has an area which is 1.9 times the carboxylate carbon peak area. This agrees well with the stoichiometric ratio between carboxylic carbon and alkyl carbons (1 : 2). **The additional peak at 284.7 eV is**

assigned to a decomposition species, most likely a H_xCN surface species, which is not beam-induced and does not increase with increasing coverage. The peak at 398 eV in the N 1s spectra is assigned to the same decomposition species. The main N 1s peak at BE 399.8/7 eV for D and L-serine (at saturation coverage) is associated with the neutral NH_2 group forming a bond with a surface copper atom. It shifts towards slightly higher BE (400.0 eV) at lower coverages. Large changes occur in the O 1s spectra as the coverage of either enantiomer increases (Figure 4(a)). At all coverages the main peak is observed around 531.4 eV. Narrow O 1s peaks at this BE have been observed for a number of amino acids on Cu surfaces and are assigned to the two oxygen atoms of the de-protonated carboxylate group, each forming a bond with a Cu atom [42, 45, 24, 27]. For low coverage, up to about 0.3 ML, a shoulder at the low BE side (530.8 eV) is observed, which is assigned to the β-OH group [54, 28]. The area ratios between the main peak and the shoulder are 2.5 and 2.2 for L- and D-serine, which is close to the expected ratio of 2 : 1. The low BE indicates that this oxygen atom is also bound to the substrate resulting in an overall μ_4 configuration with three side groups of the chiral center involved in substrate interactions (amino, carboxylate and β-OH). When the coverage approaches saturation, the low BE shoulder disappears and a new peak appears at 532.8 eV, with area ratios of 2.1 and 2.4 for L- and D-serine. This BE is typical for β-OH groups not bound to the metal surface, as in the case for serine on Cu{110} [49]. Based on this BE shift we conclude that the β-OH group is not bound to the surface for the higher coverage, which leads to a μ_3 substrate bond. The transition occurs for both enantiomers at similar coverage and appears to be driven by the fact that the μ_3 substrate bond has a smaller footprint than the low-coverage μ_4 bond, hence, the surface can accommodate more molecules [28].

In contrast to the XPS data the NEXAFS data show strong enantiomeric differences at room temperature. The carbon K-edge NEXAFS spectra of low-coverage and saturated chemisorbed layers of L and D-serine show sharp resonances at 289 eV originating from

the unoccupied carboxylate π-orbitals (see Figure 5). The measured angular dependence was used to determine the orientation of the molecules as described in section 2 [42, 8, 24, 27]. In the data sets for the saturated layers of both serine enantiomers on Cu{531}^{S} (Figure 6(c),(d)) the intensity reaches a non-zero minimum, which indicates, that the molecules assume at least two orientations. The behavior is similar to glycine and alanine on Cu{531}, which occupy adsorption sites on {311} and {110} micro facets with two different orientations [24, 27]. The data sets for both enantiomers at half saturation (0.26 and 0.30 ML) and saturation coverage were fitted allowing two orientations, characterized by the angles α_1 and α_2 with respect to the $[1\overline{1}2]$ direction (see Figure 1) and variable relative occupations. The fit results are included in the graphs of Figure 6. At saturation coverage (μ_3-bond) the orientation angles of the two enantiomers differ by about 5° ($\alpha_1 = -28/-23°$; $\alpha_2 = +31/+35°$ for L/D-serine) with similar occupation for both orientations ($A_1 : A_2 = 1.1/0.9$, see Fig. 6(c),(d)). For the low-coverage μ_4-configuration, however, there is a clear preference for only one orientation and the enantiomeric difference between the orientations of the majority species is significantly greater (Fig. 6(a),(b)). The data for D-serine show that all molecules are oriented with $\alpha_1 = 24°$. The preferred orientation of L-serine ($\alpha_1 = -9°$) is assumed by 68% of the molecules. It is rotated by $-33°$ with respect to the D-enantiomer and by $+28°$ with respect to the minority orientation ($\alpha_2 = -37°$). The comparison of these experimental results with DFT model calculations for the same system shows that the μ_4-configuration has de-protonated β-OH and carboxylate groups while the β-OH group is intact in the μ_3-configuration [28]. The preferred adsorption geometries are depicted in Figure 7.

4 Serine on Au-covered Cu{531}

Chemical modification of Cu{531} is achieved by depositing gold layers of 1 and 2 ML thickness. The formation of Au-Cu surface alloys has been observed for low coverages

of gold on close-packed copper surfaces at room temperature. At higher coverages de-alloying takes place resulting in a completely Au-terminated surface due to the lower surface energy of gold [55, 56, 57, 58, 59].

4.1 Serine on 1 ML Au/Cu{531}

Quantitative LEED-IV analysis and Au 4f surface core level shifts confirm that the first layer of gold on Cu{531} is pseudomorphic with the Au atoms essentially in the positions expected for the next layer of Cu atoms in a bulk-terminated surface [60]. The Au 4f spectrum of 1.0 ML Au/Cu$\{531\}^S$ at the bottom of Figure 8(a) shows a duplet of narrow peaks at BE 84.19 eV and 87.86 eV for Au $4f_{7/2}$ and Au $4f_{5/2}$, respectively, which indicate identical chemical environments of all gold atoms. **Note that the {531} surface is far from being close-packed, with interatomic distances within the same layer greater than 1.7 times the bulk nearest neighbor distance. A coverage of 1 ML corresponds to one Au atom per unit cell (cf Figure 1), which allows enough space for an epitaxial layer despite the 13 % larger diameter of Au compared to Cu atoms.**

The bottom spectra of Figures 9(a),(b),(c) show O 1s, C 1s and N 1s spectra of saturated chemisorbed layers of D and L-serine on 1.0 ML Au/Cu$\{531\}^S$ after adsorption at room temperature and annealing to around 350 K. When serine is adsorbed at 300 K a strong signal from a zwitterionic species with a prominent N 1s peak around BE 402 eV (NH_3) is observed (not shown). This species partly desorbs and partly converts into anionic serine after annealing to above 340 K. For this layerthere are only small BE differences of less than 0.1 eV observed between the spectra for D- and L-serine, similar to the pure surface (see Fig. 4). Also the O 1s and N 1s spectra are very similar to the corresponding spectra of serine on the pure Cu$\{531\}^S$ surface. In particular, they show peaks at the same binding energies, 399.6 eV (N 1s), 531.4 eV and 532.9 eV (O 1s), which are the signature of the μ_3-configuration with Cu-bonded amino and deprotonated carboxylate

groups and a non-bonding intact β-OH group. The ratio between the low and high BE peak is lower than for the clean surface, 1.6 for L and 1.9 for D-serine, but close enough to the expected ratio of 2 : 1 to conclude that a μ_3-configuration is assumed by the majority of molecules. **The main difference between the N 1s spectra for serine on the pure and on the gold-covered surface is the absence of a decomposition signal (397.7 eV) indicating that the presence of gold makes the surface less reactive at this temperature.** The C 1s spectra in Figure 9(b) are significantly different from those of the saturated chemisorbed layers on the **pure Cu{531} surface (Figure 4)**, mainly due to a greater chemical shift between the α and β carbon atoms, which are associated with peaks at 286.4 eV and 285.0 eV, while the peak due to the carboxylate atoms is still at 288.0 eV.

The O 1s spectra for 35% of saturation coverage of D-serine (second spectrum from bottom in Figure 9(a)) show the β-O peak at the lower BE 530.9 eV, indicating a μ_4-configuration. It is, however, not clear whether separation occurs for this layer into gold islands with higher local Au coverage and serine islands on pure Cu{531} patches. We therefore concentrate on saturated serine layers in the following discussion.

Figures 10(a),(b) show the angular dependence of the π-resonance in the C-NEXAFS spectra for saturated chemisorbed layers of D and L-serine adsorbed on 1.0 ML Au/Cu{531}. The data show very little variation as a function of the in-plane polarization angle, which is only compatible with multiple orientations, otherwise a clear minimum or maximum should be observed within this angular range. If we assume two orientations ({311} and {110} microfacets, like on the clean Cu{531} surface) the lack of significant variation implies that these must be 90° apart with identical relative coverages, however it is not possible to locate the exact values for the orientation angles α_1 and α_2 by fitting the data. L-serine shows some angular variation ($\pm$20%), which allows the determination, albeit with a relatively large error bar. The angles found are $-45° \pm 10°$ and $36° \pm 10°$, corresponding to the {311} and {110} microfacets, respectively. For D-serine it was not

possible to determine the absolute values of the orientation angles. Therefore α_1 was kept at a value close to that for L-serine, $-46°$, which leads to a value of $+46°$ for α_2. Molecules with the two orientations exist on the surface in equal amounts.

The Au 4f $_{7/2}$ signal shows chemical shifts of 0.16 and 0.20 eV, respectively, towards the higher binding energies after the adsorption of D and L-serine. This is about half of the surface core level shift typically found for gold surfaces [61] and indicates a significant interaction between serine and the Au atoms. It is, therefore, likely that the gold atoms are involved in one of the surface bonds formed by the molecules.

4.2 Serine on 2 ML Au/Cu{531}

When two monoatomic layers of gold are deposited on Cu{531} the LEED pattern shows a significantly higher background than for one layer. **The Au 4f lines are significantly broadened and can each be fitted with two peaks, which are associated with the first and second gold layer (cf bottom spectrum in Figure 8.b). This indicates that the second layer of gold-atoms is not pseudomorphic anymore and a Stranski-Krastanov-like growth mode is assumed in this regime [60]. From the data it is not clear whether the first layer is still pseudomorphic.** The experiments were performed for 2.2 ML Au/Cu{531}. The saturated chemisorbed layers of both molecules were prepared by adsorbing at 300 K and annealing to 350 K - 370 K. The O 1s and N 1s spectra of L-serine and D-serine are, again, very similar (see Fig. 9(a),(c)), except for a significant shift of 0.2 eV between the N 1s peak positions of the two enantiomers. The O 1s and N 1s spectra are also similar to those of the pure and the 1 ML Au covered Cu{531}^{S} surface. Differences in the C 1s spectra, compared to the pure surface and 1 ML Au are caused by an even greater chemical shift between the signals from the α and β carbon atoms (see Fig. 9(b)). Overall, the experimental XPS data indicate again a μ_3 bond geometry of both enantiomers on 2.2 ML Au/Cu{531}.

The angular dependence of the π-resonances in the C-NEXAFS spectra for saturated

chemisorbed layers are shown in Figures 10(d),(e). The diagrams are clearly different from those for 1 ML Au with pronounced minima around 90°, in particular for L-serine. Fitting the data with two orientations shows that one orientation, α_2, is clearly preferred over the other. 74% of the L-serine molecules on 2.2 ML Au/Cu{531} occupy an adsorption site which is characterized by an orientation angle of $\alpha_2 = 18°$ with respect to the $[1\overline{1}\overline{2}]$ direction. This is significantly different from the angles found for molecules adsorbed on {110} microfacets on the clean or the 1 ML Au-covered surface. Obviously, the presence of gold atoms has a strong influence on the adsorption geometry, which becomes also apparent from the core level shift in the Au 4f signal. The broadened Au $4f_{7/2}$ peaks observed for the clean 2.2 ML Au layer (bottom of Fig. 8(b)) merge into a single narrow peak at 84.33 eV when D-serine is adsorbed, which corresponds to BE shifts of −0.21 and +0.25 eV. **This is a strong indication that all gold atoms are in contact with the molecules at saturation coverage, otherwise surface core level shifts would still be observed for the un-covered portion of the gold atoms.**

The orientation angle of the majority species (67%) of D-serine, $\alpha_2 = 12°$, is similar to the angle determined for the L enantiomer but the orientation of the minority is very different, −61° vs −32°. The Au 4f spectra are identical for the two serine enantiomers and indicate a significant interaction between the molecules and the gold atoms in both cases.

5 Temperature dependence

5.1 TPD

Enantiospecific differences with respect to the adsorption geometries of D and L-serine are also reflected in differences in the decomposition behavior of the two enantiomers. In temperature-programmed desorption experiments on the pure surface molecular desorption was only observed for multilayers adsorbed at 300 K or below. For the chemisorbed

layers only decomposition products were recorded. Figures 11(a) and (b) show the partial pressures of the main decomposition products, H_2 (mass 2) and CO_2 (mass 44) as function of annealing temperature for low-coverage and saturated layers of D and L-serine adsorbed on the pure Cu$\{531\}^R$ surface. The differences between the enantiomers are subtle but significant. For the saturated layers both spectra show sharp peaks, which are less than 5 K wide, at slightly different temperatures for the L (441 K) and the D enantiomer (445 K). XPS experiments (see below) show that these peaks correspond to the dissociation of the molecules on the surface. The onset of hydrogen evolution starts significantly earlier for L-serine, at 396 K, with a broad desorption feature between 430 K and 460 K, which matches the desorption spectrum of the low-coverage layer (Fig. 11(a)). For D-serine, on the other hand, H_2 desorption is only observed above 415 K but extends to higher temperatures as compared to the L enantiomer. The onset of the CO_2 partial pressure is at 395 K for the saturated D-serine layer and at 415 K for L-serine, which is a behavior almost opposite that of H_2. Note, that the TPD experiments, like the LEED experiments, were carried out on a Cu$\{531\}^R$ surface, i.e the surface had the opposite chirality to that used for XPS and NEXAFS. Therefore the serine enantiomers have to be inverted for a comparison with the XPS data below.

The different decomposition behavior is even more pronounced in the N 1s XP spectra of the two enantiomers. The low BE peak around 398 eV is a marker for the H_xCN decomposition product [62], which is present in small amounts at room temperature but becomes the dominant species during the decomposition process accompanied by hydrogen desorption. The spectra in Figure 12(a) were recorded after the sample was annealed to the specified temperatures. They clearly show that the decomposition starts already below 407 K for D but not for L-serine; around 455 K the ratio between the high BE and low BE peaks shows that the decomposition has progressed much more for the D-serine layer. This is even more obvious from Figure 12(b) where the intensity of the low BE peak is plotted vs annealing temperature.

The results of similar annealing experiments for serine on 1 ML Au/Cu{531} are also plotted in Figure 12(b). They show essentially the same enantiospecific behavior with somewhat higher intensities of the decomposition peaks. The presence of gold on the surface appears to favor the H_xCN decomposition species.

6 Discussion and Conclusions

The NEXAFS results show a very significant variation in adsorption geometries and enantiomeric differences as a function of gold coverage. Preferences for certain adsorption geometries are driven by a balance between the chemical interaction with the substrate and conformational strain. Both depend on the number of surface bonds and the type of micro facet. Figure 7 and Table 1 show significant structural differences between the low-coverage μ_4 adsorption geometries of the two enantiomers on the clean surface. These lead to very substantial differences in the adsorption energies and eventually to different preferred adsorpion sites. The enantiomeric differences in the local μ_3 geometries at high coverage appear much smaller. Here only two side groups, the carboxylate (COO) and amino group (NH_2), form bonds with the substrate, which reduce the conformational strain. The third interaction through hydrogen bonds involving the β-OH group affects the molecular orientation much less than a bond to the substrate. There are, however, enantiomeric differences in the long-range order, which are mediated through these hydrogen bonds. Those differences in the degree of hydrogen bonding are also the most likely cause for the enantiomeric differences observed in the thermal decomposition behavior and do, therefore affect the surface chemistry of the system. Note, hydrogen bonding is not fully included in the DFT calculations quoted in Figure 7 and Table 1. They were carried out for the lower coverage of 0.25 ML where the interaction between the molecules is limited [28].

When the top-most layer of atoms in the Cu{531} surface (i.e. the kink atoms) is

replaced by Au, the orientation of the serine molecules changes dramatically. Although the absolute orientation cannot be determined with high accuracy, the difference angle between the two orientations is defined much more accurately. In the special case of D-serine, where $\alpha_2 \approx \alpha_1 + 90°$, the sum of the two π-resonance intensities is the same for all polarization angles, irrespective of the actual values of α_1 and α_2. It is, therefore intrinsically impossible to quantify enantiomeric differences in the molecular orientation by NEXAFS, however the thermal decomposition behavior (see Fig. 12(b)) gives a very clear indication that they exist. Given that the XPS spectra indicate a μ_3 bond configuration for saturation coverage and a similar involvement of all gold atoms, the arrangements should, in principle, be similar to the μ_3 geometries depicted in Figure 7 with the gold atoms replacing the top-layer copper atoms. Lateral shifts of the gold atoms and/or the molecular side groups due to changes in the relative bond strengths can lead rotations of the order of 10° as observed experimentally.

The second layer of gold is not pseudomorphic, which is reflected in the very different molecular orientations on the 2.2 ML Au/Cu{531} surface compared to 1 ML Au. Again, the XPS spectra indicate that all surface Au atoms interact with the molecules in a μ_3 bond configuration, however substantial deviations from a bulk-terminated pseudomorphic substrate geometry have to be considered. Very substantial enantiomeric differences are seen in the orientation of the minority species ($-32°$ vs $-61°$), the origin of which is not clear yet. The exact arrangement of atoms in these structures can only be clarified experimentally by using diffraction or forward-focussing techniques or theoretical modeling.

In summary, we show through a combination of synchrotron-based XPS and NEXAFS and DFT that both enantiomers of serine adsorb on the clean intrinsically chiral Cu{531} surface in μ_4 geometries (with de-protonated β-OH groups) at low coverage and in μ_3 geometries at saturation coverage. Significantly larger enantiomeric differences are seen for the μ_4 geometries, which involve substrate bonds of three side groups of the chiral center,

i.e. a three-point interaction. The μ_3 adsorption geometry, where only the carboxylate and amino groups form substrate bonds and the β-OH group is involved in inter-molecular interactions, leads to smaller but still significant enantiomeric differences, both in geometry and the decomposition behavior. When Cu{531} is modified by the deposition of 1 ML and 2 ML Au the orientations of serine at saturation coverage are significantly different. In all cases, however, a μ_3 bond coordination is found (at saturation) involving different numbers of Au atoms, which leads to relatively small enantiomeric differences.

Acknowledgement

The research leading to these results has received funding from the European Community's Seventh Framework Programme (FP7/2007-2013) under grant agreement No. 226716, through the Marie Curie Early Stage Training Network "MONET" (No. MEST-CT-2005-020908) and the EPSRC. The authors would also like to acknowledge the support during the experiments provided by the staff of BESSY II, in particular D. Batchelor and thank S. J. Jenkins and A. Ievins for making the results of their DFT calculations available.

References

[1] L. H. Easson and E. Stedman, Biochem. J. **27** (1933) 1257.

[2] V. A. Davankov, Chirality **9** (1997) 99.

[3] G. Proctor, *Asymmetric Synthesis*, Oxford University Press (1997).

[4] A. Baiker, J. Mol. Catal. A **115** (1997) 473.

[5] A. Baiker, J. Mol. Catal. A **163** (2000) 205.

[6] A. J. Gellman, J. D. Horvath and M. T. Buelow, J. Mol. Catal. A **167** (2001) 3.

[7] G. A. Attard, J. Phys. Chem. B **105** (2001) 3158.

[8] G. Held and M. J. Gladys, Top. Catal. **48** (2008) 128.

[9] A. J. Gellman, ACS Nano **4**(1) (2010) 5, pMID: 20099908.

[10] G. A. Attard, A. Ahmadi, J. Feliu, A. Rodes, E. Herrero, S. Blaise and G. Jerkiewicz, J. Phys. Chem. B **103** (1999) 1381.

[11] C. F. McFadden, P. S. Cremer and A. J. Gellman, Langmuir **12** (1996) 2483.

[12] S. J. Jenkins and S. Pratt, Surf. Sci. Rep. **62** (2007) 373.

[13] J. D. Horvath and A. J. Gellman, J. Am. Chem. Soc. **123** (2001) 7953.

[14] J. D. Horvath and A. J. Gellman, J. Am. Chem. Soc. **124** (2002) 2384.

[15] J. D. Horvath, A. Koritnik, P. Kamakoti, D. S. Sholl and A. J. Gellman, J. Am. Chem. Soc. **126** (2004) 14988.

[16] Y. Huang and A. J. Gellman, Catal. Lett. **125**(3-4) (2008) 177.

[17] A. Ahmadi, G. A. Attard, J. Feliu and A. Rodes, Langmuir **15** (1999) 2420.

[18] R. M. Hazen and D. S. Sholl, Nature Mat. **2** (2003) 367.

[19] Z. Sljivancanin, K. V. Gothelf and B. Hammer, J. Am. Chem. Soc. **124** (2002) 14789 .

[20] R. Fasel, J. Wider, C. Quitmann, K.-H. Ernst and T. Greber, Angew. Chem. Int. Ed **43** (2004) 2853.

[21] B. Bhatia and D. S. Sholl, Angew. Chem. Int. Ed. **44** (2005) 7761.

[22] T. Greber, Z. Sljivancanin, J. Wider and B. Hammer, Phys. Rev. Lett. **96** (2006) 056103.

[23] G. Jones, S. J. Jenkins and D. A. King, Surf. Sci. **600** (2006) L224.

[24] M. J. Gladys, A. V. Stevens, N. R. Scott, G. Jones, D. Batchelor and G. Held, J. Phys. Chem. C **111** (2007) 8331.

[25] B. Bhatia and D. S. Sholl, J. Chem. Phys. **128** (2008) 144709.

[26] J. N. James and D. A. Sholl, Curr. Opinion Colloid Interface Science **13** (2008) 60.

[27] T. Eralp, Z. V. Zheleva, A. Shavorskiy, V. R. Dhanak and G. Held, Langmuir **26** (2010) 10918.

[28] T. Eralp, A. Ievin, A. Shavorskiy, S. J. Jenkins and G. Held, submitted .

[29] T. D. Power, A. Asthagiri and D. S. Sholl, Langmuir **18** (2002) 3737.

[30] S. R. Puisto, G. Held, V. Ranea, S. J. Jenkins, E. E. Mola and D. A. King, J. Phys. Chem. B **109** (2005) 22456 .

[31] G. Jones, M. J. Gladys, J. Ottal, S. J. Jenkins and G. Held, Phys. Rev. B **79** (2009) 165420.

[32] D. I. Sayago, M. Polcik, G. Nisbet, C. L. A. Lamont and D. P. Woodruff, Surf. Sci. **590** (2005) 76.

[33] C. S. Fadley, *Synchrotron Radiation Research: Advances in Surface Science*, Vol. chap. 9, Plenum Press, New York (1992) .

[34] D. P. Woodruff and A. M. Bradshaw, Rep. Prog. Phys. **57** (1994) 1029.

[35] D. P. Woodruff, Surface Science Reports **62** (2007) 1.

[36] H. Bonzel, Progress in Surface Science **42**(1-4) (1993) 219 .

[37] T. D. Power and D. S. Sholl, J. Vac. Sci. Technol. A **17** (1999) 1700.

[38] B. Bhatia and D. S. Sholl, J. Chem. Phys. **122** (2005) 204707.

[39] S. M. Barlow and R. Raval, Surf. Sci. Rep. **50** (2003) 201.

[40] M. Forster, M. S. Dyer, M. Persson and R. Raval, J. Am. Chem. Soc. **131** (2009) 10173.

[41] C. J. Baddeley and G. Held, *Chiral Molecules on Surfaces*, Comprehensive Nanoscience and Technology, Elsevier, Amsterdam, 1. ed. (2010).

[42] J. Hasselström, O. Karis, M. Weinelt, N. Wassdahl, A. Nilsson, M. Nyberg, L. G. M. Petterson, M. G. Samant and J. Stöhr, Surf. Sci. **407** (1998) 221.

[43] M. Polcik, F. Allegretti, D. I. Sayago, G. Nisbet, C. L. A. Lamont and D. P. Woodruff, Phys. Rev. Lett. **92** (2004) 236103.

[44] S. M. Barlow, S. Louafi, D. Le Roux, J. Williams, C. Muryn, S. Haq and R. Raval, Surf. Sci. **590** (2005) 243.

[45] G. Jones, L. B. Jones, F. Thibault–Starzyk, E. A. Seddon, R. Raval, S. J. Jenkins and G. Held, Surf. Sci. **600** (2006) 1924.

[46] F. Gao, Z. Li, Y. Wanga, L. Burkholder and W. T. Tysoe, J. Phys. Chem. C **111** (2007) 9981.

[47] F. Gao, Z. Li, Y. Wang, L. Burkholder and W. T. Tysoe, Surf. Sci. **601** (2007) 3276.

[48] F. Gao, Y. Wang, L. Burkholder and W. T. Tysoe, Surf. Sci **601** (2007) 3579.

[49] T. Eralp, A. Shavorskiy, Z. V. Zheleva, G. Held, N. Kalashnyk, Y. Ning and T. R. Linderoth, Langmuir **26** (2010) 18841.

[50] T. Eralp, A. Shavorskiy and G. Held, Surf. Sci. **605** (2011) 468.

[51] J. Stöhr, *NEXAFS spectroscopy*, Springer Series in Surface Sciences, Springer, Berlin, 2. ed. (1996).

[52] J. Nyberg, M. Hasselström, O. Karis, N. Wassdahl, M. Weinelt, A. Nilsson and L. G. M. Petterson, J. Chem. Phys. **112** (2000) 5420.

[53] T. Eralp, *Fundamental Enantiospecific Interactions of Amino Acids on Metal Surfaces*, Phd thesis, University of Reading (2010).

[54] R. M. Petoral and K. Uvdal, Journal of Electron Spectroscopy and Related Phenomena **128** (2003) 159.

[55] P. Steiner, S. Hüfner, N. Mårtensson and B. Johansson, Solid State Communications **37** (1981) 73.

[56] M. Kuhn and T. K. Sham, Phys. Rev. B **49** (1994) 1647.

[57] D. Naumovi, A. Stuck, T. Greber, J. Osterwalder and L. Schlapbach, Surf. Sci. **269** (1992) 719.

[58] Y. G. Shen, J. Yao, D. J. O'Connor, B. V. King and R. J. MacDonald, J. of Phys.: Condens. Matter **8** (1996) 4903.

[59] A. V. Ruban, H. L. Skriver and J. K. Nørskov, Phys. Rev. B **59** (1999) 15990.

[60] Z. Zheleva, T. Eralp, A. Cornish, and G. Held, in preparation .

[61] R. Denecke and N. Mårtensson, *Adsorbate induced surface core level shifts of metals*, Vol. III/42A4 of *Landolt-Börnstein Numerical Data and Functional Relationships in Science and Technology, New Series*, Springer, Berlin, 1. ed. (2005) .

[62] A. Shavorskiy, F. Aksoy, M. E. Grass, Z. Liu, H. Bluhm and G. Held, J. Am. Chem. Soc. **133** (2011) 6659.

	α_1 (Θ_1) {311} facet		α_2 (Θ_2) {110} facet	
Clean Cu{531}				
L-Serine (52% sat)	$-9°$	(67%)		
	$-37°$	(33%)		
D-Serine (59% sat)			24°	(100%)
L-Serine (DFT 0.25 ML)	$-10°$			
D-Serine (DFT 0.25 ML)			30°	
L-Serine (100% sat)	$-28°$	(52%)	31°	(48%)
D-Serine (100% sat)	$-23°$	(49%)	35°	(51%)
1.0 ML Au / Cu{531}				
L-Serine (100% sat)	$-45°$	(49%)	36°	(51%)
D-Serine (100% sat)	$-45°$*	(53%)	46°*	(47%)
2.2 ML Au / Cu{531}				
L-Serine (100% sat)	$-32°$	(26%)	18°	(74%)
D-Serine (100% sat)	$-61°$	(33%)	12°	(67%)

Table 1: Summary of the NEXAFS results. Orientation angles $\alpha_{1,2}$ (angle between the $[1\overline{1}2]$ direction of Cu{531}^{S} and the surface-projection of the normal of the carboxylate O-C-O triangle) and relative coverages $\Theta_{1,2}$. For the pure Cu{531}^{S} surface also the DFT results from Ref [28] are included.

* Only the difference between α_1 and α_2 could be determined for D-serine on 1 ML Au/ Cu{531};the absolute value of α_1 is adjusted to match the value of L-serine.

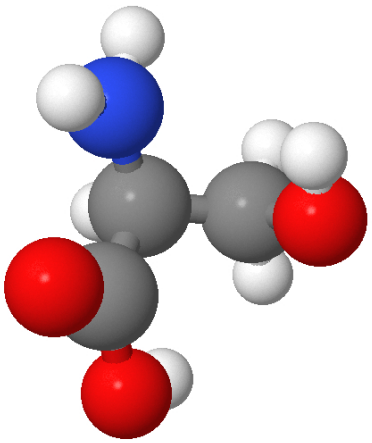

(a)

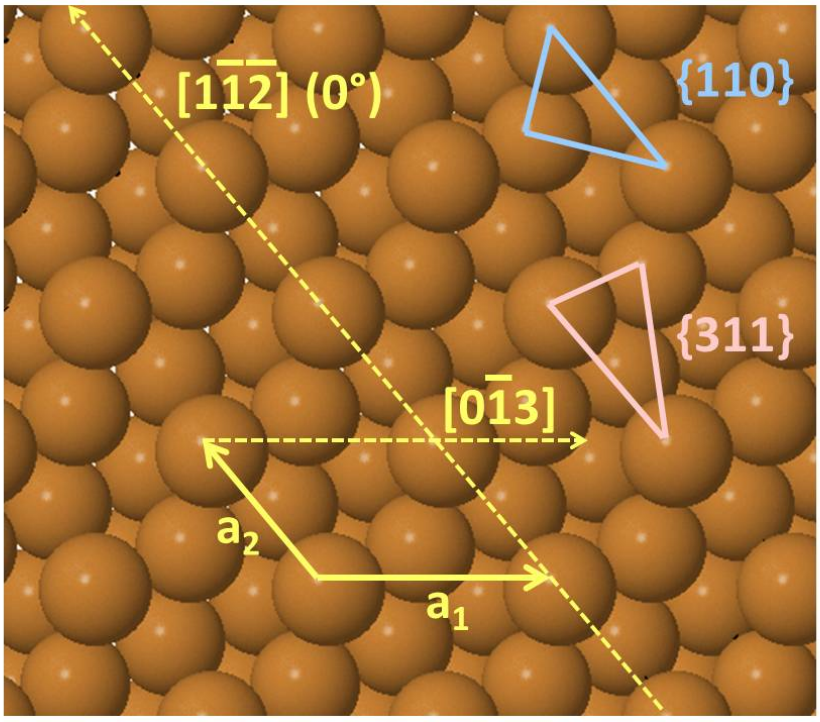

(b)

Figure 1: (a) Ball and stick model of L-serine (red = oxygen, blue = nitrogen, gray = carbon, white = hydrogen). (b) Ball model of the clean unreconstructed Cu{531}^{S} surface indicating the surface unit cell vectors and the main crystallographic directions. At the right-hind side of the diagram {110} and {311} microfacets are indicated, which consist of two first layer and one second layer Cu atom each, forming rectangular and isosceles triangles, respectively.

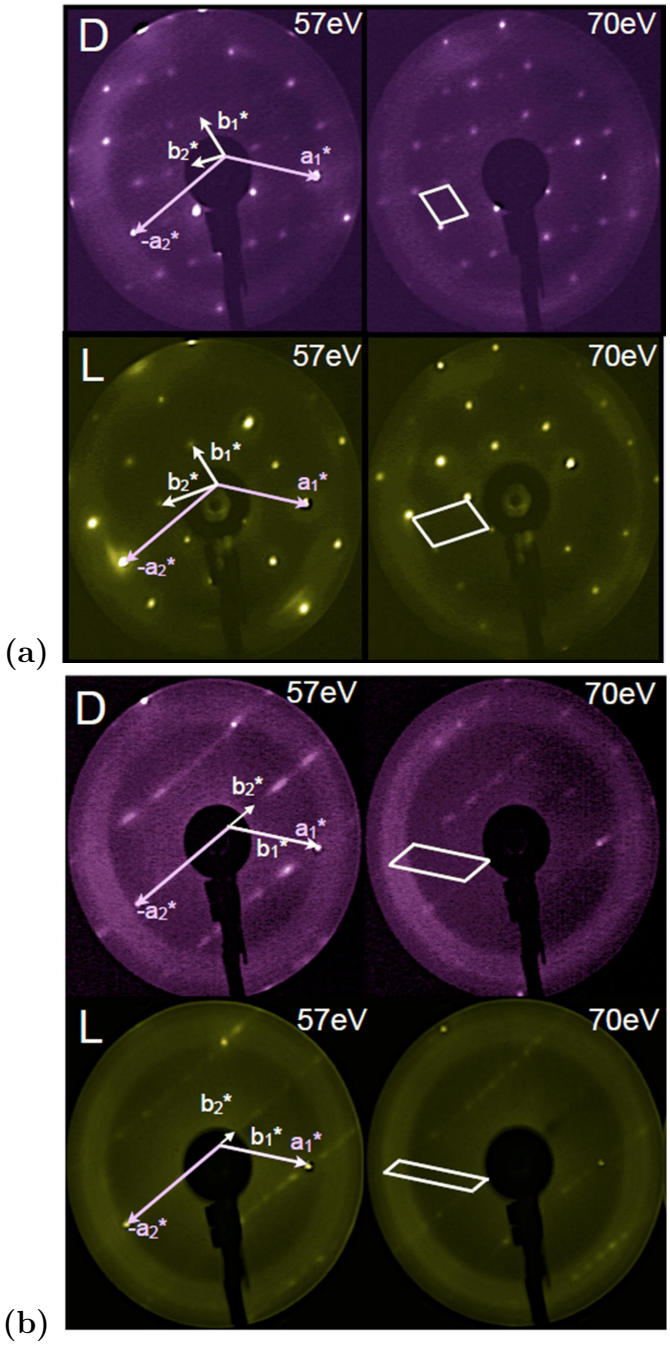

Figure 2: LEED superstructures observed at 57 eV and 70 eV for (a) 29% of saturation coverage of L-serine, 26% of saturation coverage of D-serine on Cu{531}^{R} surface; (b) 100% of the saturation coverage of L and D-serine. Clean surface (a_1* and a_2*) and overlayer (b_1* and b_2*) reciprocal unit cell vectors are shown.

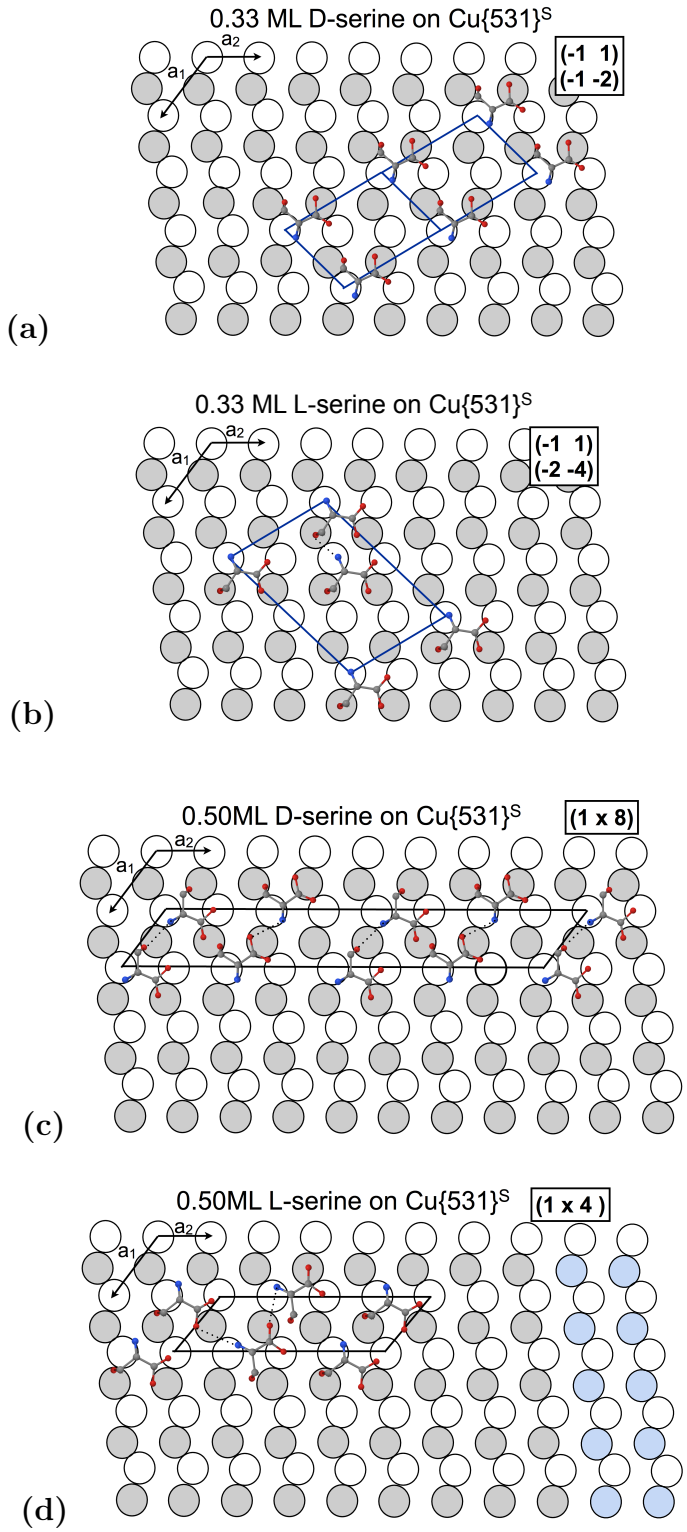

Figure 3: Schematic structure models of the low-coverage and high-coverage super-structures of L and D-serine on Cu{531}^{S}: (a) (-1 1; -2 -4) for 0.33 ML D-serine, (b) (-1 1; -1 -2) for 0.33 ML L-serine, (c) $p(1\times4)$ for 0.50 ML D-serine, and (d) $p(1\times8)$ for 0.50 ML L-serine. The surface coordination of orientation of molecules is in accordance with the spectroscopic results from XPS and NEXAFS.

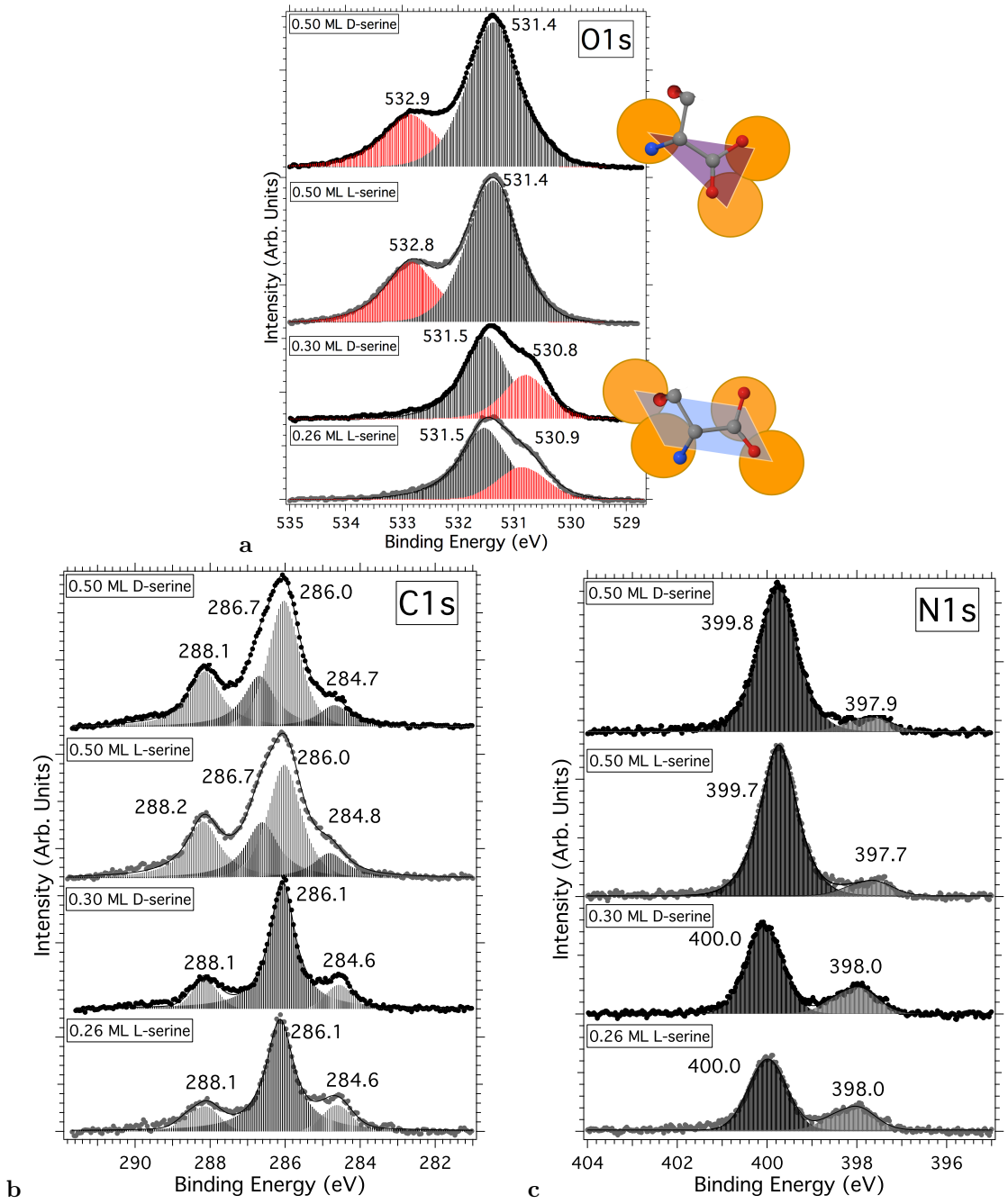

Figure 4: O 1s (a), C 1s (b), and N 1s (c) XP spectra of different coverages of L and D-serine adsorbed on the clean Cu{531}^{S} (photon energy=630 eV) [28].

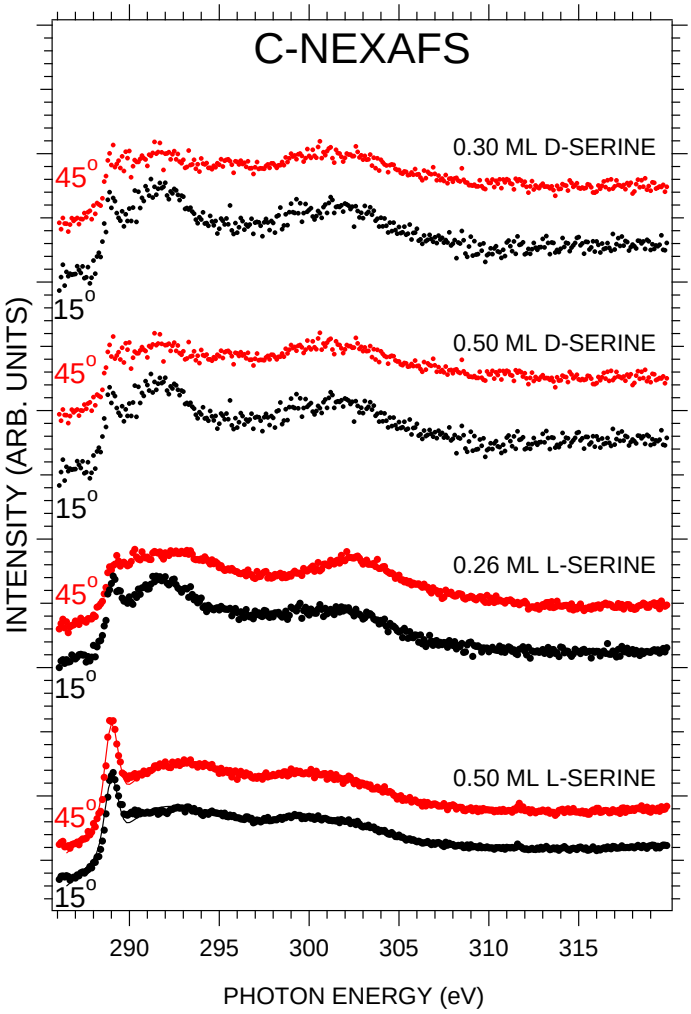

Figure 5: A selection of NEXAFS raw data collected for polarization angles of 15° and 45° for different coverages of L and D-serine adsorbed on Cu{531}^{S}.

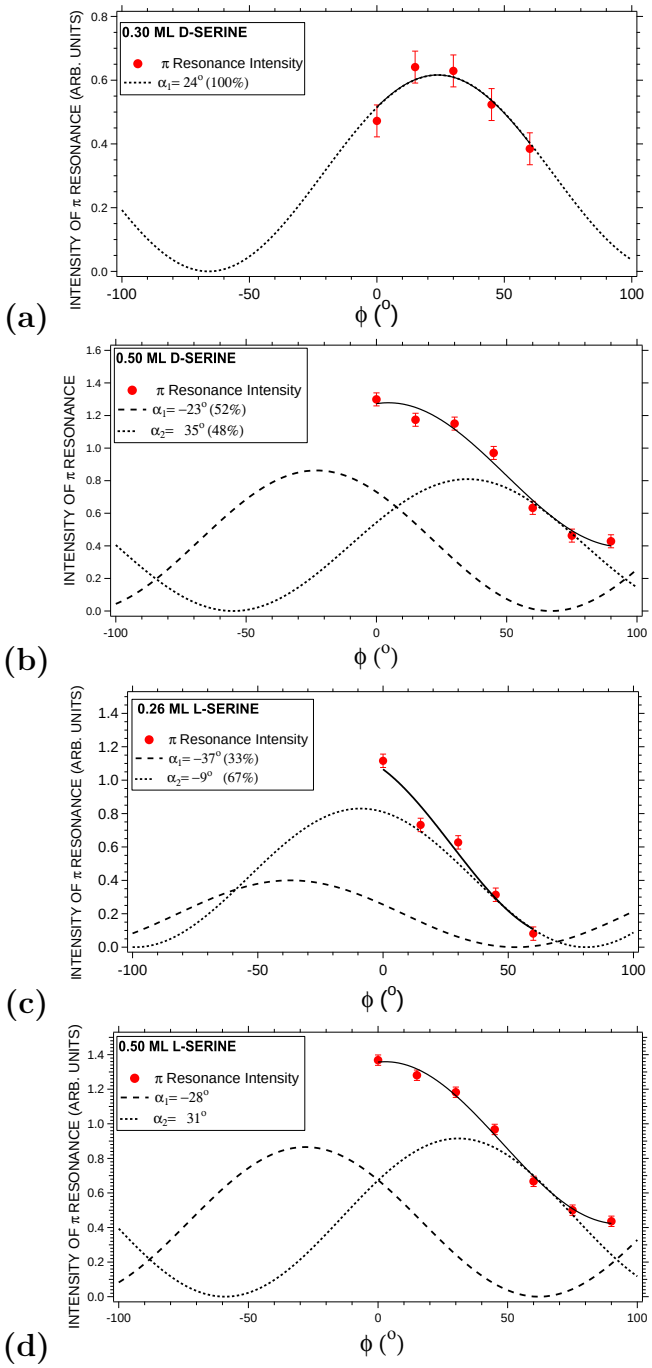

Figure 6: Angular dependence of the π-resonance in the C K-edge NEXAFS spectra for 0.30 ML D-serine (a), 0.26 ML L-serine (c) and saturation coverages (0.50 ML) of D- and L-serine on the Cu{531}^{S} surface (b, d). The fitted angular dependence (individual orientations and sum of the two curves) and the parameters $\alpha_{1,2}$ of the best fits are included in the diagrams [28].

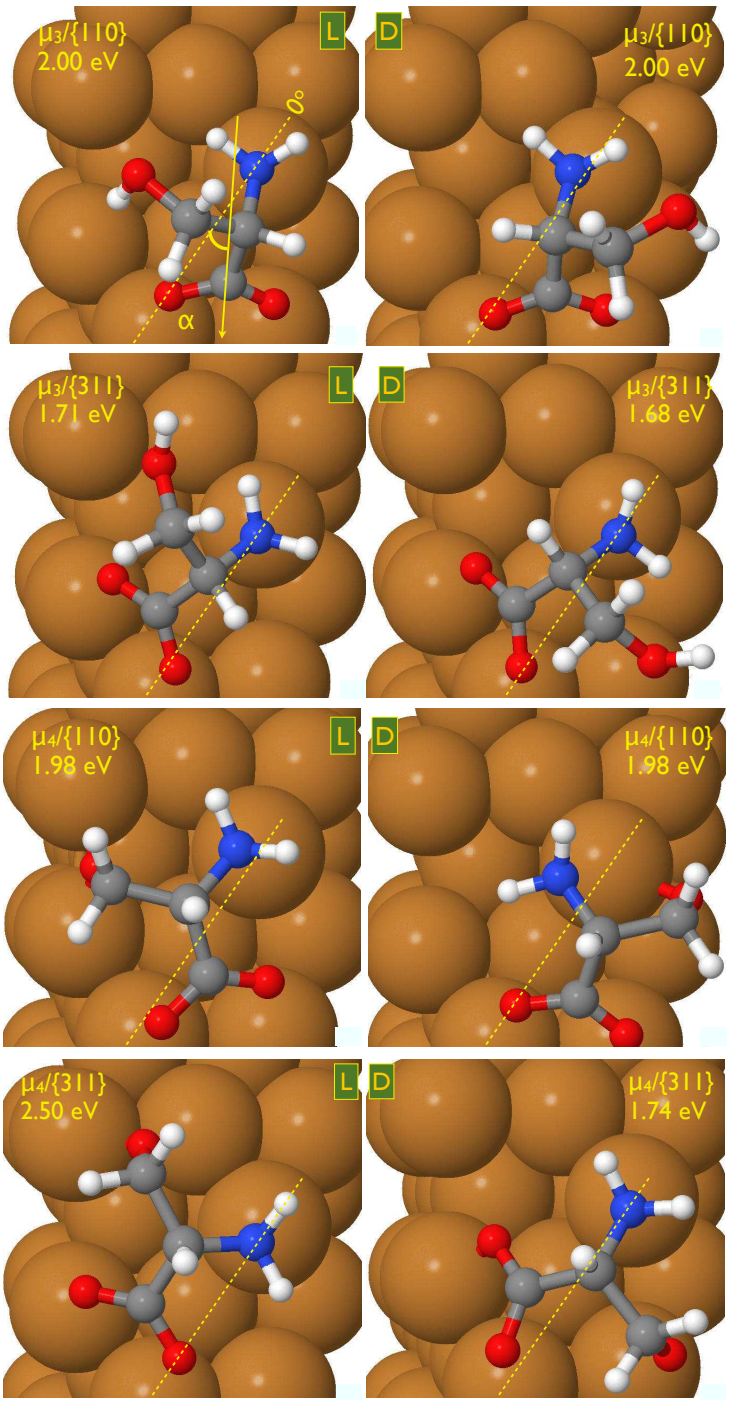

Figure 7: DFT-optimized μ_3 and μ_4 adsorption geometries for L- and D-Serine on the {110} and {311} microfacets of Cu{531}^{S}. The respective adsorption energies are indicated in the Figure; the dotted line (0°) indicates the $[1\overline{1}2]$ crystallographic direction. (red=oxygen, blue=nitrogen, gray=carbon, white=hydrogen). The μ_4 geometries with the highest adsorption energies agree well with the NEXAFS results for the majority species; the μ_3 geometries are only in qualitative agreement with NEXAFS because not all hydrogen bonds were represented in the modeling [28].

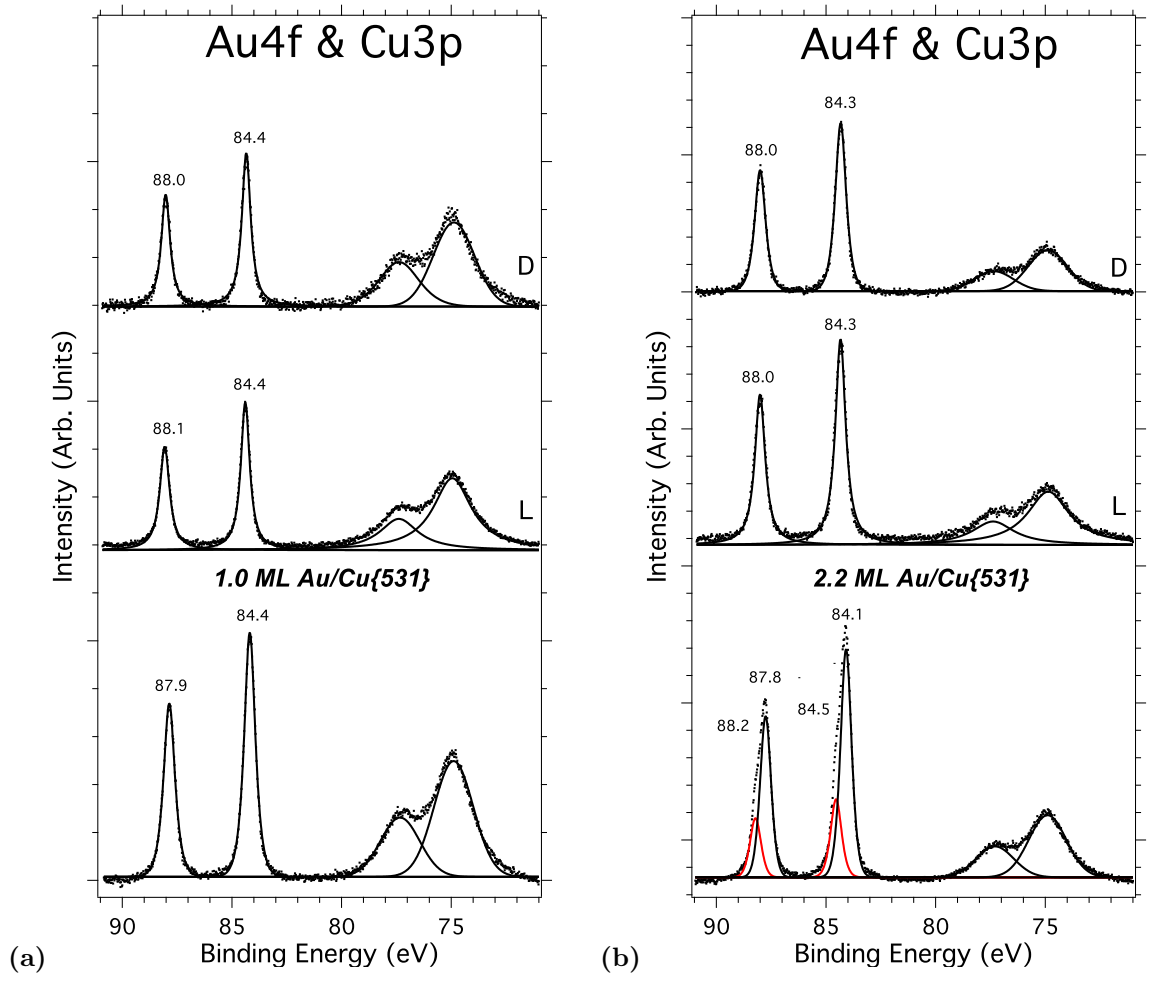

Figure 8: Au 4f and Cu 3p spectra of 1.0 ML Au/Cu{531}^{S} (a) and 2.2 ML Au/Cu{531}^{S} (b). Bottom spectra: uncovered surface, middle: saturated chemisorbed layer of L-serine, top: saturated chemisorbed layer of D-serine. (photon energy=300 eV)

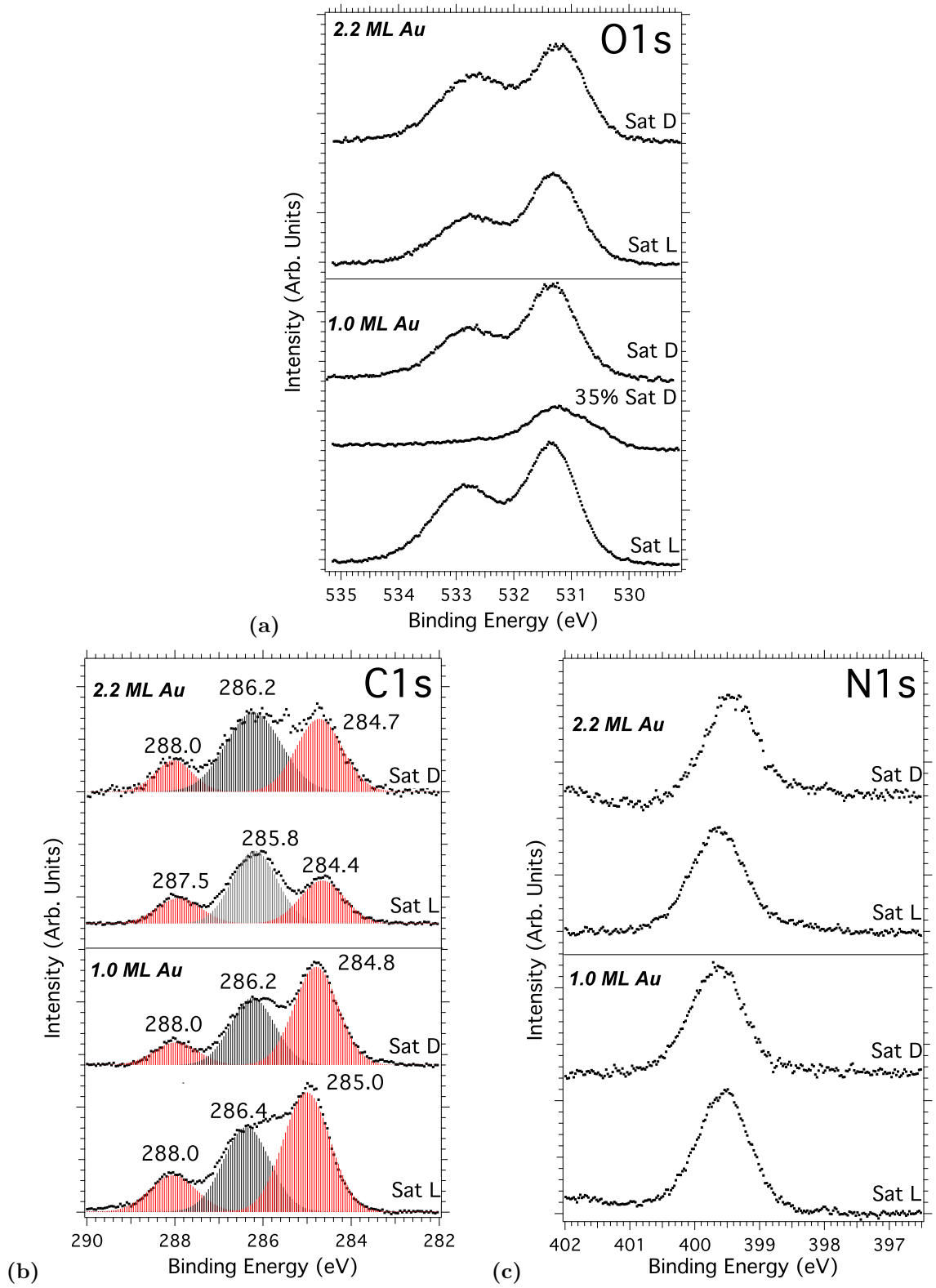

Figure 9: O 1s (a), N 1s (b), and C 1s (c) XP spectra of saturation coverages of L and D-serine on 1.0 ML and 2.2 ML Au/Cu{531}^{S}. (photon energy=630 eV). **For comparison, panel (a) also contains the O 1s spectrum of 35 % suturation coverage of D-serine (2nd spectrum from bottom).**

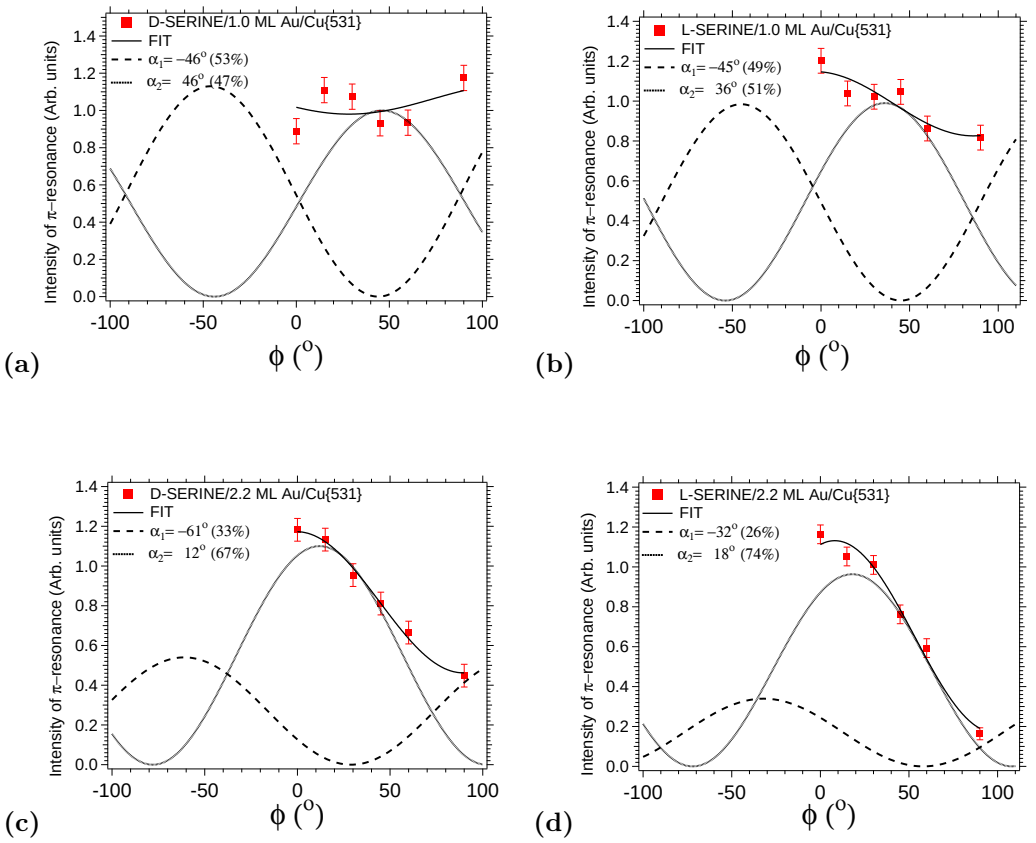

Figure 10: Angular dependence of the π-resonance in the C K-edge NEXAFS spectra for saturated chemisorbed layers of (a) D-serine on 1.0 ML Au/Cu{531}^{S}, (b) L-serine on 1.0 ML Au/Cu{531}^{S}, (c) D-serine on 2.2 ML Au/Cu{531}^{S}, L-serine on 2.2 ML Au/Cu{531}^{S}. The fitted angular dependence (individual orientations and sum of the two curves) and the parameters $\alpha_{1,2}$ of the best fits are included in the diagrams.

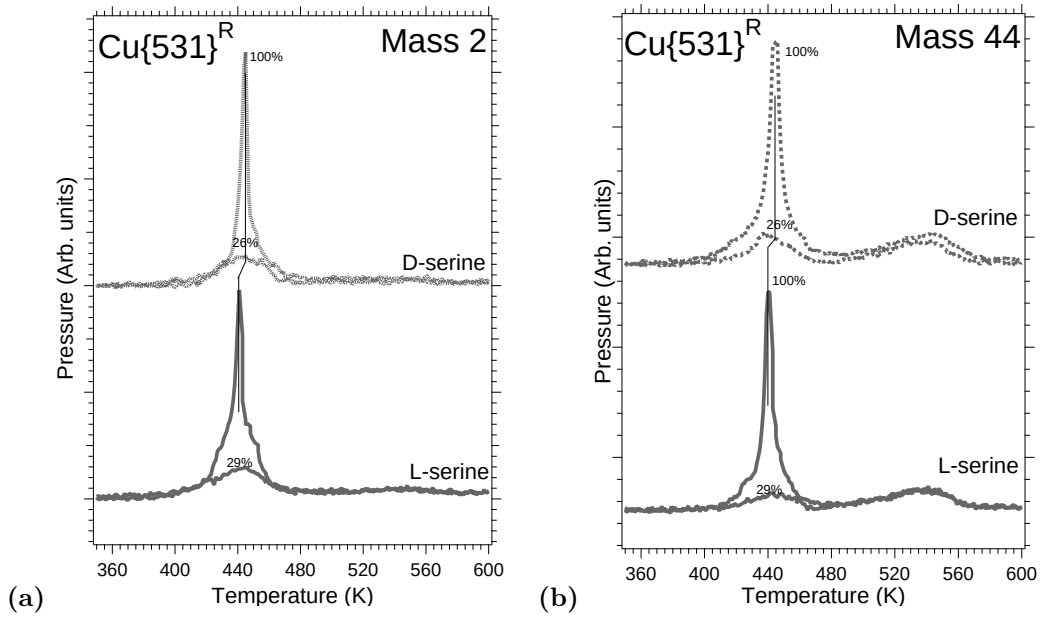

Figure 11: Mass 2, (H_2, a) and mass 44 (CO_2, b) TPD spectra of different coverages of L (29% and 100% of saturated chemisorbed layer) and D-serine (26% and 100% of saturated chemisorbed layer) on Cu{531}^{R}.

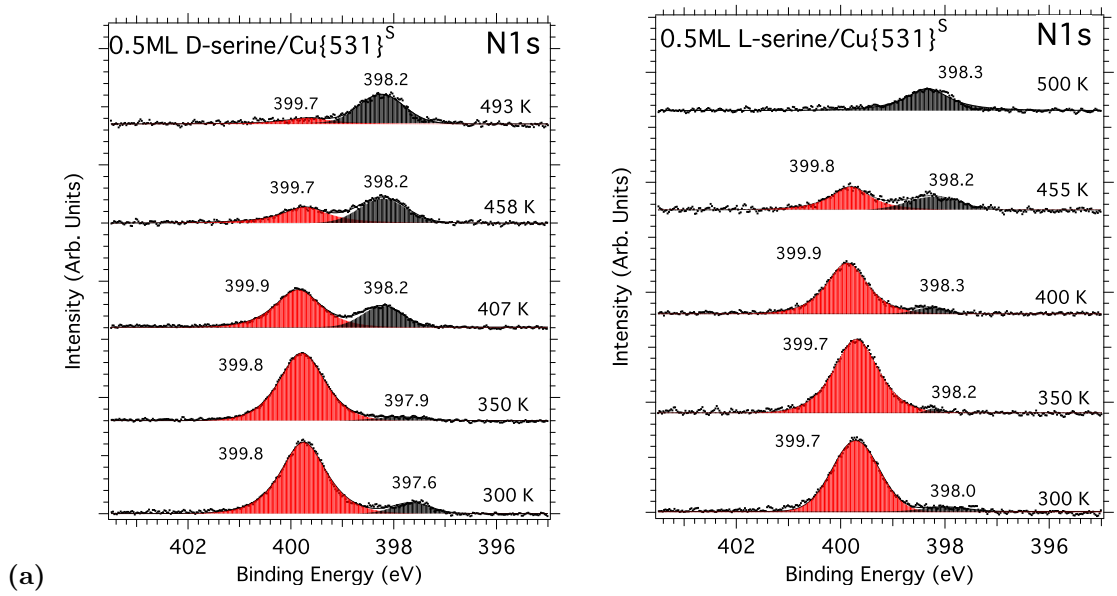

(a)

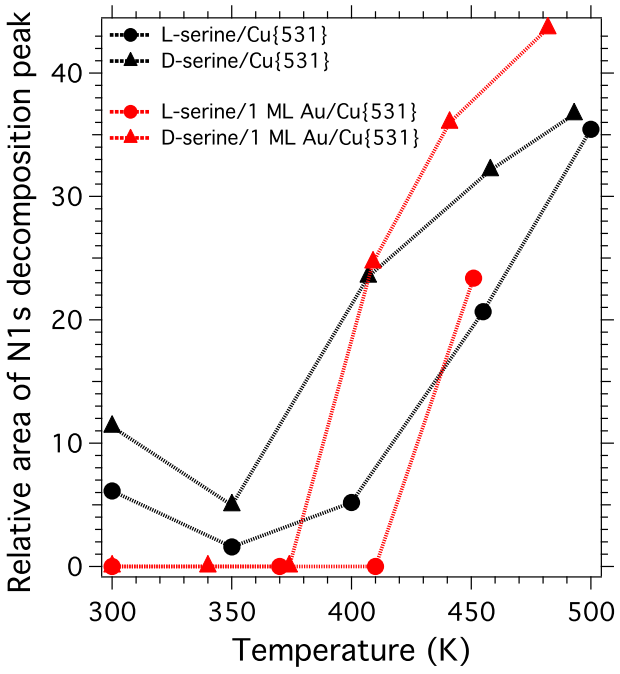

(b)

Figure 12: (a) N 1s XP spectra for saturated D and L-serine layers on pure Cu{531}^{S} after annealing to the indicated temperatures; (b) peak area associated with the CNH_x decomposition product as a function of temperature (relative to the N 1s peak area of the saturated chemisorbed layer at 350 K).